Nanoscale Anisotropic Plastic Deformation in Single Crystal Aragonite

C. Kearney,[1] Z. Zhao,[2] B. J. F. Bruet,[3] R. Radovitzky,[2] M. C. Boyce,[1] and C. Ortiz[3,*]

[1]*Department of Mechanical Engineering, Massachusetts Institute of Technology, 77 Massachusetts Avenue, Cambridge, Massachusetts 02139, USA*

[2]*Department of Aeronautics and Astronautics, Massachusetts Institute of Technology, 77 Massachusetts Avenue, Cambridge, Massachusetts 02139, USA*

[3]*Department of Materials Science and Engineering, Massachusetts Institute of Technology, 77 Massachusetts Avenue, Cambridge, Massachusetts 02139, USA*

(Received 15 February 2006; published 30 June 2006)

The nanoscale anisotropic elastic-plastic behavior of single-crystal aragonite is studied using nanoindentation and tapping mode atomic force microscopy imaging. Force-depth curves coaxial to the c axis exhibited load plateaus indicative of dislocation nucleation events. Plasticity on distinct slip systems was evident in residual topographic impressions where four pileup lobes were present after indentation with a conospherical probe and distinct, protruding slip bands were present after indentation with a Berkovich pyramidal probe. A finite element crystal plasticity model revealed the governing roles of the $\{110\}\langle 001\rangle$ slip system family, as well as the (100)[010], (100)[001], (010)[100], (010)[001], (001)[100], and (001)[010] systems.

DOI: 10.1103/PhysRevLett.96.255505 PACS numbers: 62.20.Fe

Aragonite (an orthorhombic form of calcium carbonate, $CaCO_3$) is a mineral ubiquitous in natural systems including living organisms [1,2] and geological structures [3]. Examples of the former include micrometer-sized tablets which compose ~95% of the inner nacreous layer found in mollusk shells [4,5], nanometer to micrometer-sized fibers of scleratinian stony coral skeletons [6], and spicules in some sponges [2]. Geologically, aragonite is predominantly found in the upper mantle [7]. Since the identification of the orthorhombic crystal structure of aragonite by Bragg in 1924 [8], ongoing investigations have studied a range of aspects of this mineral [3] including high pressure experiments [9], which eventually led to the identification of the calcite-to-aragonite transition and the development of the $CaCO_3$ phase diagram [10].

Although the mechanical behavior of aragonite is a critical determinant of its many biological and geological functions, only a few reports exist in this area and a fundamental mechanistic understanding is lacking. The anisotropic elastic constants were determined in 1910 [11] using bending and torsion experiments, and again recently using Brillouin spectroscopy [12]. Regarding plastic deformation, a few reports exist on similar minerals, e.g., calcite [13], which is a rhombohedral form of $CaCO_3$ and olivine [14], which, like aragonite, has an orthorhombic structure. For olivine, transmission electron microscopy (TEM) on samples deformed under high pressure showed plastic deformation to be governed by slip on several systems [14]. Large scale plastic flow of polycrystalline [15] and porous [16] aragonite has been investigated at high temperatures and pressures, identifying dislocation creep as the dominant mechanism for the former and a transition from localized brittle failure to cataclastic flow with increasing porosity and grain size for the latter. Knoop microhardness testing on single-crystal aragonite at room temperature showed anisotropic behavior when comparing the (100), (010), and (001) planes, as well as in-plane anisotropy in the (100) and (010) planes, in contrast to nearly isotropic microhardness in the (001) plane [17]. Recently, nanoindentation studies have been performed on aragonite-based scallops [18] and on individual nacre tablets [19,20] showing plastic deformation and pileup. In order to more fully understand the mechanical design principles of such natural biocomposite materials, it is essential to study the properties of the pure constituents, such as aragonite. In this Letter, the anisotropic mechanical behavior of single-crystal aragonite was studied using nanoindentation in conjunction with tapping mode atomic force microscopy (TMAFM) imaging of residual indents. The use of indenter probe tips with two different geometries (pyramidal Berkovich and conospherical) and a finite element crystal plasticity model enabled interrogation and identification of the underlying activated slip systems which govern anisotropic plasticity.

Figure 1(a) depicts averaged nanoindentation load-unload data using a Berkovich probe tip for single-crystal aragonite on three mutually orthogonal planes, where one plane is normal to the orthorhombic crystal c axis (001) and the other planes [$(\bar{1}10)$ and $(\bar{1}\,\bar{3}\,0)$] are perpendicular to the (001) plane. The force-depth curves for the three planes revealed an anisotropic nanomechanical response. An Oliver-Pharr (O-P) [21] reduction of these data [22] for a maximum load of 1000 μN gives (modulus, hardness) pairs of (102.8 ± 2.4 GPa, 6.2 ± 0.3 GPa), (100.1 ± 3.4 GPa, 4.6 ± 0.3 GPa), and (108.1 ± 2.3 GPa, 4.36 ± 0.4 GPa) for the (001), $(\bar{1}10)$, and $(\bar{1}\,\bar{3}\,0)$ planes, respectively, and indicates an anisotropic yield stress. This observed plastic anisotropy is expected to result from

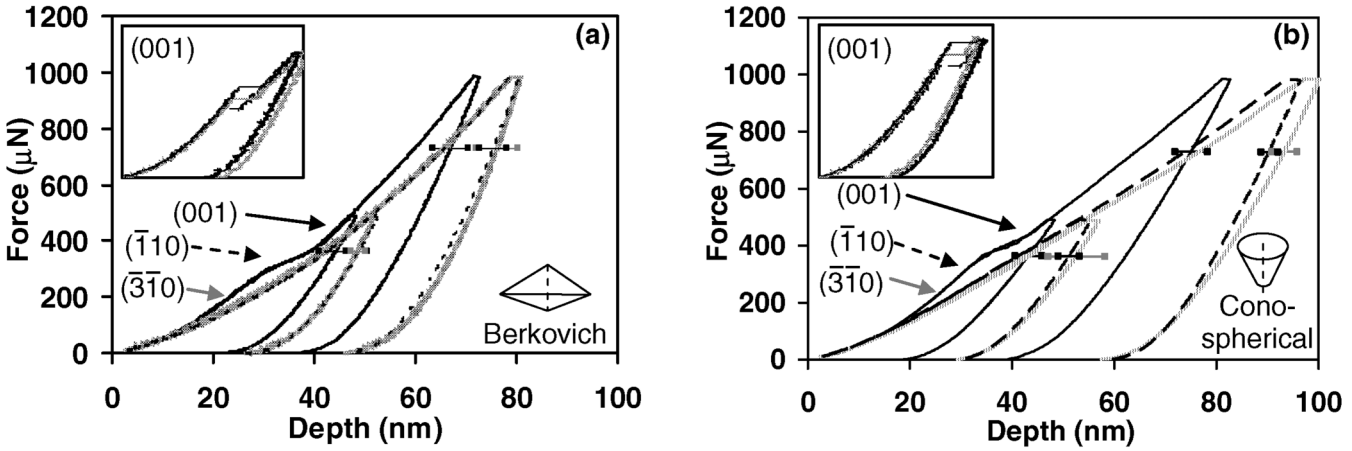

FIG. 1. Averaged force-depth data for nanoindentation normal to three mutually orthogonal planes of single-crystal aragonite (data set of 20 for each curve); loading rate of 50 μN/s; error bars indicate one standard deviation in displacement at a given force level. Insets: three representative individual curves from the (001) data sets (maximum load 500 μN, depth axis 50 nm) using a (a) Berkovich tip, (b) conospherical tip.

activation of slip on preferred slip systems which depend on the indentation direction. The (001) plane indents show a noticeable change in slope in the averaged force-depth curves at ~314 and 386 μN. The origin of this slope change is clearly seen when examining individual (as opposed to averaged) load-unload curves which display distinct load plateaus (309.0 ± 27.6 μN) [Fig. 1(a) inset]. Nanoindentation force-depth curves on a number of other materials (e.g. metals, semiconductors, and oxides) have also exhibited load plateaus [23–25]; constitutive stability criteria have been used to model these events [23,24] and attribute the plateau to the onset of dislocation nucleation. TEM revealed extensive dislocation activity after nanoindentation on ceramic single crystals (Al_2O_3, SiC) [25].

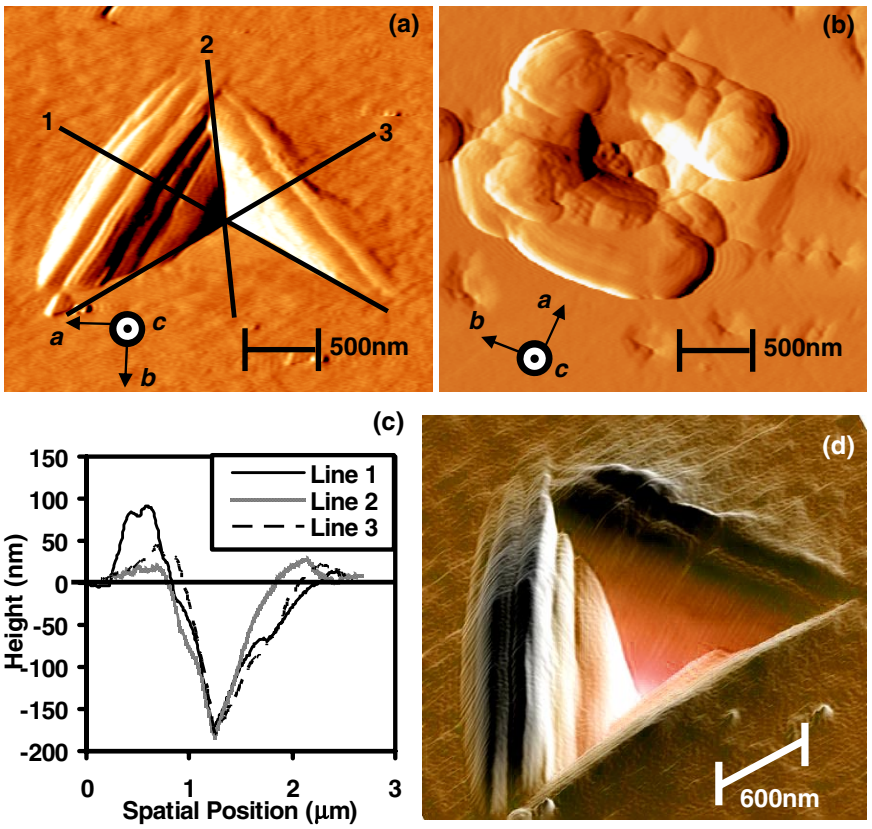

FIG. 2 (color online). TMAFM images of residual indents, (a) amplitude image, 10 mN maximum load (loaded depths of ~290 nm and residual depths of ~180 nm), Berkovich tip, load rate 1 mN/s, (b) amplitude image, 5 mN maximum load (loaded depths of ~420 nm and residual depths of ~300 nm), 1 μm, 60° conospherical tip, load rate 1 mN/s, ⊙ indicates c axis is out of the page. (c) Line profiles of Berkovich indent depicted in (a); and (d) 3D height image of Berkovich indent.

Anisotropic behavior was also observed in nanoindentation via a conospherical tip [nominal tip radius <1 μm, 60° cone, Fig. 1(b)]. An O-P reduction applied to these data for a maximum load of 1000 μN gives (modulus, hardness) pairs of (89 $\pm$ 1.8 GPa, 8.6 $\pm$ 0.36 GPa), (95 $\pm$ 2.78 GPa, 6.5 $\pm$ 0.13 GPa), and (85 $\pm$ 2.25 GPa, 6.36 $\pm$ 0.19 GPa) for the (001), $(\bar{1}10)$, and $(\bar{1}\,\bar{3}\,0)$ planes, respectively, which again highlights the yield anisotropy. As in the Berkovich indentation, there is a marked change in slope for the (001) plane data (at $\sim$381 μN to $\sim$439 μN) and the individual curves [Fig. 1(b) inset] depict the distinct load plateaus (424.4 $\pm$ 61.0 μN).

TMAFM images of residual indents after unloading from larger maximum loads [Figs. 2(a) and 2(b)] reveal a central impression and a surrounding pileup zone indicating extensive plastic deformation and no microcracking. Preferential pileup was observed for both probe tip geometries, indicating anisotropic plastic behavior. In the conospherical indent, the pileup was localized predominantly in four lobes around the indenter. For the Berkovich tip, pileup was typically adjacent to two sides of the indenter and showed directionally biased protruding striations that appear to be slip bands. Line profiles [Fig. 2(c)] together with 3D atomic force microscope images of the Berkovich pileup [Fig. 2(d)] further highlight the banded nature of the pileup.

A finite element model was employed to simulate the anisotropic plastic response of single-crystal aragonite for the two indenter geometries. Based on the clear experimental evidence of slip-dominated plastic activity, the overarching assumptions associated with the kinematics of plastic slip in crystals [26] are postulated as the governing deformation mechanism and a crystal plasticity model [27,28] is adopted to describe the constitutive response of aragonite. This type of model is well established in the simulation of anisotropic plastic behavior in metals [28,29] where the operative slip systems of the crystal as well as their resistance and hardening properties are known. In this work, since the slip systems in aragonite are largely unknown, the model is used to interrogate and identify the operative systems required to explain the observed indentation slip and pileup patterns produced by both the conospherical and Berkovich probe tips. The slip resistance of all slip systems is assumed to be the same. The computed pileup patterns were qualitatively insensitive to the slip resistance value. Simulations assuming the $\{100\}\langle 001\rangle$ family of slip systems as suggested by prior investigations [15,16] failed to produce the observed residual topographic impressions. The four pileup lobes observed experimentally for the conospherical indentation [Fig. 2(b)] exhibit a twofold symmetry with an aspect ratio similar to the lattice constants ratio a/b, suggesting pileups may result from slip activity on $\{110\}\langle 001\rangle$ systems. Following this observation and previous work on olivine [which shares with aragonite the orthorhombic structure [14]], the six systems of the $\{110\}\langle 001\rangle$ family were added to the set of cubic slip systems postulated initially. When the resulting set of 12 slip systems is considered, the simulation reproduces the observed pileup pattern [Fig. 3(a)], thus indicating that the proposed slip systems provide a plausible kinematic mechanism explaining the observed anisotropic plastic behavior.

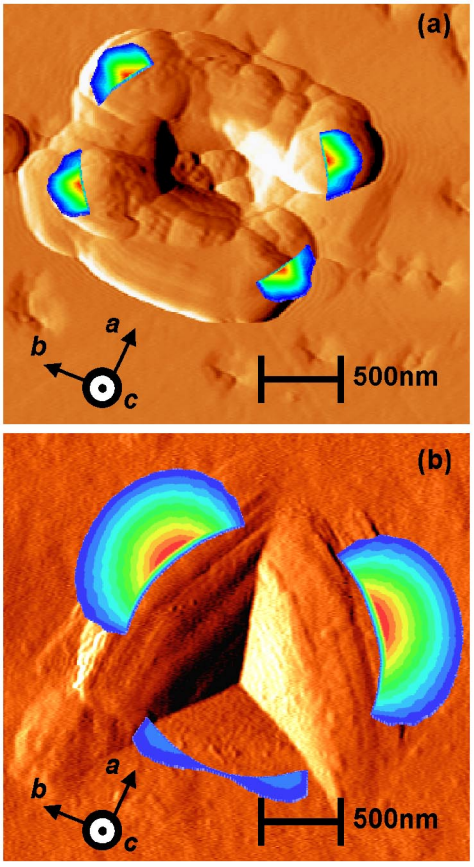

FIG. 3 (color online). Simulated pileup pattern compared to experimental TMAFM amplitude images. Blue color is minimum, red is maximum (a) conospherical tip, (b) Berkovich tip; pileups take place at two sides with (110)[001] and $(\bar{1}10)$[001] dominant.

In order to provide further support for the postulated operative slip systems, the same model was used to simulate the indentation with the Berkovich probe tip. The nonsymmetric geometry of the Berkovich tip further exposes the anisotropy of plastic deformation and provides a stringent test of the model's ability to describe the basic mechanisms of anisotropic plastic flow. Figure 3(b) compares the pileup patterns obtained numerically with the corresponding experimental observations. The (110)[001] and $(\bar{1}10)$[001] slip systems are found to provide the kinematic mechanisms of plastic slip necessary to produce the pileup bands observed in the Berkovich residual impression, thus supporting the postulated slip systems in aragonite. Furthermore, the gradient in magnitude of slip activity

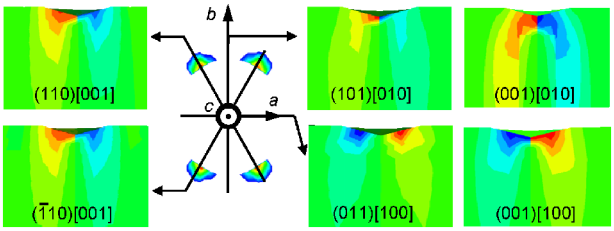

FIG. 4 (color online). Through thickness cross sections depicting contours of slip activity in indicated slip systems for conospherical nanoindentation predicted by the model (red color is maximum positive slip, blue color is maximum negative slip, and green color is unslipped region).

is consistent with the slope of the banded region observed in the line profile.

The mechanisms governing the formation of pileups for the conospherical probe tip indentation are described in more detail in a series of cross-sectional views (Fig. 4) which document the through-thickness distribution of slip activation within the indentation zone predicted by the model. The (100) plane cross sections shown on the top right figures exhibit activation of slip on the (101)[010] and (001)[010] systems whereas the (010) plane cross sections shown on the bottom right figures exhibit activation of slip on the (011)[100] and (001)[100] systems. Activation of slip in these systems leads to shearing of the material away from the indentation zone along the [010] and [100] directions, respectively. This slip activity is kinematically compatible with the activation of the (110)[001] and $(\bar{1}10)[001]$ slip systems which are responsible for the pileup along the [001] direction.

This previously unreported detail of the nanoscale anisotropic plastic behavior of aragonite contributes to our understanding of mechanical design of biological composites, geological behavior, and development of biomimetic materials. In particular, given that brittle failure is averted in micron and submicron scaled biological composite structures due to the small length scale effect [2,5], the hardness values reported here indicate that natural composites containing small-scale aragonite structures (e.g., tablets in the nacre of seashells) are able to withstand high stress prior to yield. Furthermore, this study details specific aspects of anisotropic plasticity in aragonite where the preferentially oriented crystallographic structure of biological composites is considered to play an important functional role [30].

This research was supported by the U.S. Army through the MIT Institute for Soldier Nanotechnologies, under Contract No. DAAD-19-02-D0002. The authors thank the MIT CMSE, and A. Schwartzman and the MIT Nanomechanical Technology Laboratory. R. R. and Z. Z. acknowledge support of the U.S. Department of Energy (DOE W-7405-ENG-48, B523297).

*Email address: cortiz@mit.edu

[1] H. A. Lowenstam and S. Weiner, *On Biomineralization* (Oxford University Press, New York, 1989).
[2] S. A. Wainwright, W. D. Biggs, J. D. Currey, and J. M. Gosline, *Mechanical Design in Organisms* (Wiley, New York, 1976).
[3] R. J. Reeder, *Reviews in Mineralogy: Volume 11*, Carbonates: Mineralogy and Chemistry (Bookcrafters, Inc., Chelsea, MI, 1983).
[4] J. D. Taylor, W. J. Kennedy, and A. Hall, Bull. Br. Mus. (Nat. Hist.) Zool. **3**, 1 (1969).
[5] A. P. Jackson, J. F. V. Vincent, and R. M. Turner, Proc. R. Soc. Lond. B **234**, 415 (1988).
[6] W. H. Bryan and D. Hill, Proc. R. Soc., Queensl. **52**, 78 (1941).
[7] S. Ono, T. Kikegawa, Y. Ohishi, and J. Tsuchiya, Am. Mineral. **90**, 667 (2005).
[8] W. L. Bragg, Proc. R. Soc. A **105**, 16 (1924).
[9] P. W. Bridgman, Am. J. Sci. **237**, 7 (1939).
[10] K. Suito *et al.*, Am. Mineral. **86**, 997 (2001).
[11] W. Voigt, in *Lehrbuch der Kristallphysik* (B. G. Teubner, Leipzig, 1910).
[12] L-G. Liu, C.-C. Chen, C-C. Lin, and Y.-J. Yang, Phys. Chem. Miner. **32**, 97 (2005).
[13] N. L. Carter, Rev. Geophys. Space Phys. **14**, 301 (1976).
[14] C. B. Raleigh, J. Geophys. Res. **73**, 5391 (1968).
[15] E. Rybacki *et al.*,, J. Geophys. Res. **180**, 1 (2003).
[16] J. Renner and F. Rummel, Tectonophysics **258**, 151 (1996).
[17] Y. H. Han, H. Li, T. Y. Wong, and R. C. Bradt, J. Am. Ceram. Soc. **74**, 3129 (1991).
[18] X. Li and P. Nardi, Nanotechnology **15**, 211 (2004).
[19] B. J. F. Bruet *et al.*, J. Mater. Res. **20**, 2400 (2005).
[20] X. Li *et al.*, Nano Lett. **4**, 613 (2004).
[21] W. C. Oliver and G. M. Pharr, J. Mater. Res. **19**, 3 (2004).
[22] The (modulus, hardness) pairs estimated here should be regarded as ''apparent'' since the O-P model assumes isotropy [21].
[23] W. W. Gerberich *et al.*, Acta Mater. **44**, 3585 (1996).
[24] K. J. Van Vliet *et al.*, Phys. Rev. B **67**, 104105 (2003).
[25] T. F. Page, W. C. Oliver, and C. J. McHargue, J. Mater. Res. **7**, 450 (1992).
[26] J. R. Rice, J. Mech. Phys. Solids **19**, 433 (1971).
[27] D. Pierce, R. J. Asaro, and A. Needleman, Acta Metall. **31**, 1951 (1983).
[28] S. R. Kalidindi, C. A. Bronkhorst, and L. Anand, J. Mech. Phys. Solids **40**, 537 (1992).
[29] Y. Wang, D. Raabe, C. Kluber, and F. Roters, Acta Mater. **52**, 2229 (2004).
[30] S. Weiner, I. Sagi, and L. Addadi, Science **309**, 1027 (2005).